Earth and Planetary Science Letters 427 (2015) 136–148

Contents lists available at ScienceDirect

Earth and Planetary Science Letters

www.elsevier.com/locate/epsl

Silicate weathering in the Ganges alluvial plain

Patrick J. Frings [a,*], Wim Clymans [a], Guillaume Fontorbe [a], William Gray [b], Govind J. Chakrapani [c], Daniel J. Conley [a], Christina De La Rocha [d,1]

[a] Department of Geology, Lund University, Sölvegaten 12, 223 62, Lund, Sweden
[b] Department of Earth Science and Marine Science Institute, University of California, Santa Barbara, CA 93106, USA
[c] Department of Earth Sciences, Indian Institute of Technology, Roorkee, India
[d] IUEM, CNRS UMR 5639, University of West Brittany, Plouzané, France

ARTICLE INFO

Article history:
Received 17 February 2015
Received in revised form 20 June 2015
Accepted 24 June 2015
Available online 16 July 2015
Editor: M. Frank

Keywords:
silicon isotopes
silicate weathering
dissolved silica
Ganges
lowland weathering

ABSTRACT

The Ganges is one of the world's largest rivers and lies at the heart of a body of literature that investigates the interaction between mountain orogeny, weathering and global climate change. Three regions can be recognised in the Ganges basin, with the Himalayan orogeny to the north and the plateaus of peninsular India to the south together delimiting the Ganges alluvial plain. Despite constituting approximately 80% of the basin, weathering processes in the peninsula and alluvial plain have received little attention. Here we present an analysis of 51 water samples along a transect of the alluvial plain, including all major tributaries. We focus on the geochemistry of silicon and its isotopes. Area normalised dissolved Si yields are approximately twice as high in rivers of Himalaya origin than the plain and peninsular tributaries (82, 51 and 32 kmol SiO_2 km^{-2} yr^{-1}, respectively). Such dissolved Si fluxes are not widely used as weathering rate indicators because a large but variable fraction of the DSi mobilised during the initial weathering process is retained in secondary clay minerals. However, the silicon isotopic composition of dissolved Si (expressed as $\delta^{30}Si$) varies from +0.8‰ in the Ganges mainstem at the Himalaya front to +3.0‰ in alluvial plain streams and appears to be controlled by weathering congruency, i.e. by the degree of incorporation of Si into secondary phases. The higher $\delta^{30}Si$ values therefore reflect decreasing weathering congruency in the lowland river catchments. This is exploited to quantify the degree of removal using a Rayleigh isotope mass balance model, and consequently derive initial silica mobilisation rates of 200, 150 and 107 kmol SiO_2 km^{-2} yr^{-1}, for the Himalaya, peninsular India and the alluvial plain, respectively. Because the non-Himalayan regions dominate the catchment area, the majority of initial silica mobilisation from primary minerals occurs in the alluvial plain and peninsular catchment (41% and 34%, respectively).

1. Introduction

On geological timescales, Earth's climate is regulated by a balance between silicate weathering reactions that consume atmospheric CO_2 and a continuous input of carbon from volcanic and metamorphic degassing (Walker et al., 1981). Given that degassing rates vary on long timescales but climate has remained broadly stable, a negative feedback between the rate of CO_2 removal and atmospheric CO_2 concentrations must exist (Berner and Caldeira, 1997). The dependency of silicate weathering rates on climate is the strongest contender for such a feedback, although the exact nature of this dependency remains elusive. River geochemistry is an integrative function of catchment solute inputs and biogeochemical cycling, and so is an excellent tool with which to quantify and understand weathering rates, provided inputs of solutes from non-silicate sources, biological cycling and human activity can be successfully de-convolved.

Driven by the hypothesis that the long-term global cooling since the early Eocene, illustrated, for example, by marine sediment records (Zachos et al., 2001) can be attributed to the Himalayan orogenesis over the same period (Raymo and Ruddiman, 1992), many investigations focus on the major and trace element and isotope geochemistry of the mountainous headwaters of large rivers. As weathering processes in these regions become better understood their role as important long-term CO_2 sinks is increasingly questioned due to their apparently modest silicate weathering rates and small surface areas (see e.g. Moore et al., 2013). However, there is also a growing awareness that lowland regions

* Corresponding author.
E-mail address: patrick.frings@geol.lu.se (P.J. Frings).
[1] Presently no affiliation.

http://dx.doi.org/10.1016/j.epsl.2015.06.049

of large rivers potentially play an important role in the generation of river weathering fluxes. The deposition and active reworking of freshly eroded and highly weatherable material in a system with water and sediment residence times substantially longer than the upstream source areas creates potential for additional silicate weathering and CO_2 consumption (Bouchez et al., 2012; Lupker et al., 2012). Unfortunately, the capacity of the lowland regions to modify weathering fluxes at the whole-basin scale is poorly understood. For example, the Ganges is one of the world's largest river systems, lies at the heart of the uplift-climate hypothesis (Raymo and Ruddiman, 1992), and has a vast alluvial plain in the foreland basin of the Himalaya. Yet few studies have attempted to budget silicate weathering in the alluvial plain although it constitutes the majority of the Ganges basin. Those that have are often complicated by the anthropogenically perturbed solute and sediment budgets, or the presence of evaporite soils (Rengarajan et al., 2009).

Examination of the biogeochemical cycling of silicon (Si) can provide insights into weathering processes in the Ganges alluvial plain (hereafter 'GAP') because Si derives ultimately – and exclusively – from silicate minerals. Indeed, the flux of dissolved Si (DSi) from a catchment has often been used as a surrogate for silicate weathering rates (Edmond and Huh, 1997; Rengarajan et al., 2009; White and Blum, 1995). However, DSi fluxes are not widely used since a large but variable amount of DSi mobilised during solubilisation of primary minerals typically ends up locked into clay minerals or cycling biologically, meaning what is observed in a river does not necessarily directly reflect the initial weathering. If we are to quantify weathering fluxes, the information we really want is the rate at which Si is mobilised from primary minerals, before some fraction of it is incorporated into secondary clays and biogenic silica. This could be further converted into a silicate–cation weathering rate if the Si/cation ratio of the parent material is known (although the fraction of silicate hydrolysis driven by inorganic acids and the fraction of silicate-hosted cations incorporated into secondary clays must be accounted for by other methods). Previous work on Si geochemistry in the Ganges basin has focused mostly on the behaviour of Si isotopes in the upper end of the basin (Fontorbe et al., 2013), or in groundwater of the Ganges–Brahmaputra delta (Georg et al., 2009); knowledge of Si geochemistry and its relation to silicate weathering in the GAP is limited.

Here, based on samples from 51 sites in the Ganges basin, we use an approach that exploits the fractionation of silicon isotopes during removal of Si from solution to constrain initial DSi mobilisation rates. Our results show that a majority of initial Si mobilisation occurs in lowland regions of the catchment, albeit at lower surface area-normalised rates than the Himalaya. Overall, this suggests that any role the Himalayan orogeny plays as a driver and determinant of global climate change has been modulated by the evolution and functioning of its alluvial plains over time.

2. Study area

The Ganges (Fig. 1) drains a basin of $\sim 0.98 \times 10^6$ km^2 and has a mean annual discharge in Bangladesh of $\sim 490 \times 10^9$ m^3 yr^{-1}. Conventionally the Ganges basin is subdivided into three broad physiographic regions: the Himalayan orogeny to the north, the hills and plateaus of Peninsular India to the south, with the GAP lying between. Climate within the Ganges basin varies widely, from tropical/sub-tropical in the south to areas with sub-zero mean annual temperatures in the high Himalaya (Tripathy and Singh, 2010). The most important hydrological aspect is the annual monsoon which occurs progressively from the southwest between approximately June and September and provides ~80% of the rainfall in the basin (Dalai et al., 2002; Tripathy and Singh, 2010). Rainfall is not evenly divided between the three regions; the Himalaya have average runoff of ~100 cm yr^{-1}, Peninsular India ~30 cm yr^{-1} and the GAP ~46 cm yr^{-1}.

Ganges catchment streams draining the Himalaya are well studied (e.g. Bickle et al., 2003; Chakrapani, 2005; Dalai et al., 2002; Fontorbe et al., 2013; Galy and France-Lanord, 1999) and are generally characterised by rapid physical and chemical erosion rates, weathering fluxes dominated by carbonate weathering and minor contributions from silicate weathering and hot springs. Besides the headwaters of the Ganges itself, major tributaries draining into the Ganges from the Himalayan orogeny include the Yamuna, Ramganga, Ghaghara (also known as the Karnali), the Gandak (the Narayani) and the Kosi. The Himalaya account for 17% of the total surface area of the basin, and 34% of total runoff, and are thought to supply ~44% of dissolved Si (Galy and France-Lanord, 1999).

The southern part of the Ganges basin partly drains a plateau of the Bundelkhand crystalline granites and Vindhyan Precambrian, shales, sandstones and sedimentary carbonates. Together, they constitute a peripheral cratonic bulge that forms part of the Indian shield. The south–western basin also partly drains the Deccan Traps, solidified flood basalts from the late Cretaceous. The shield is relatively low-elevation and is covered in part by deeply weathered soils (laterites) as well as saline and alkaline soils. As a result, the headwaters of southern tributaries of the Ganges have different chemistries compared to the Himalayan streams, e.g. their cation compositions are often dominated by Na^+ (Rengarajan et al., 2009) instead of Ca^{2+}. Major rivers draining peninsular India include the Chambal, Betwa and Ken, tributaries to the Yamuna with their headwaters in the Deccan Traps, and the Tons (also known as the Tamas) and the Son (the Sone) (Fig. 1). Peninsular India accounts for ~31% of the Ganges basin surface area, and 19% of the runoff. Galy and France-Lanord (1999) estimate that peninsular catchments supply ~30% of total exported DSi.

The GAP is essentially the result of the infilling of the active foreland basin by fluvial sediments, of both Himalayan and cratonic origin, up to several kilometres thick. The ~300 km wide GAP lies in a south-easterly direction and consists of massive beds of clays, sand and gravels, mostly Himalayan, and currently aggrades by $\sim 65 \times 10^6$ tons yr^{-1} (Sinha, 2005). It is a region of low elevation, limited topography and high population density. Many streams drain the GAP directly; the largest of these is the 900 km long Gomati (also referred to as the Gomti), which originates ~50 km from the Himalaya and drains an interfluve between the Ramganga and the Ghaghara. Other notable tributaries include the Punpun from the south and the Buri Gandak from the north. The GAP accounts for 52% of the total surface area of the Ganges basin. The alluvial plain supplies about 33% of total Ganga discharge and ~26% of DSi (Galy and France-Lanord, 1999), and disproportionately contribute Na, Cl and Sr (Rai et al., 2010).

An unusual feature of the GAP is the presence of saline/alkali soil salts and carbonates, locally called *kankar*, that are thought to form through repeated annual wetting and drying of depressions or seasonally endorheic areas. Locally, they can strongly influence the water chemistry but their composition is poorly constrained (Galy and France-Lanord, 1999; Rengarajan et al., 2009; Sarin et al., 1989). Large-scale human activity has altered the hydrology of the region through irrigation, including the construction of canals, groundwater abstraction and damming for hydropower or water management, although this is still somewhat limited in scope.

3. Materials and methods

3.1. Fieldwork

Samples were collected at 51 sites within the Ganges fluvial network, including 19 on the Ganges mainstem itself. They span

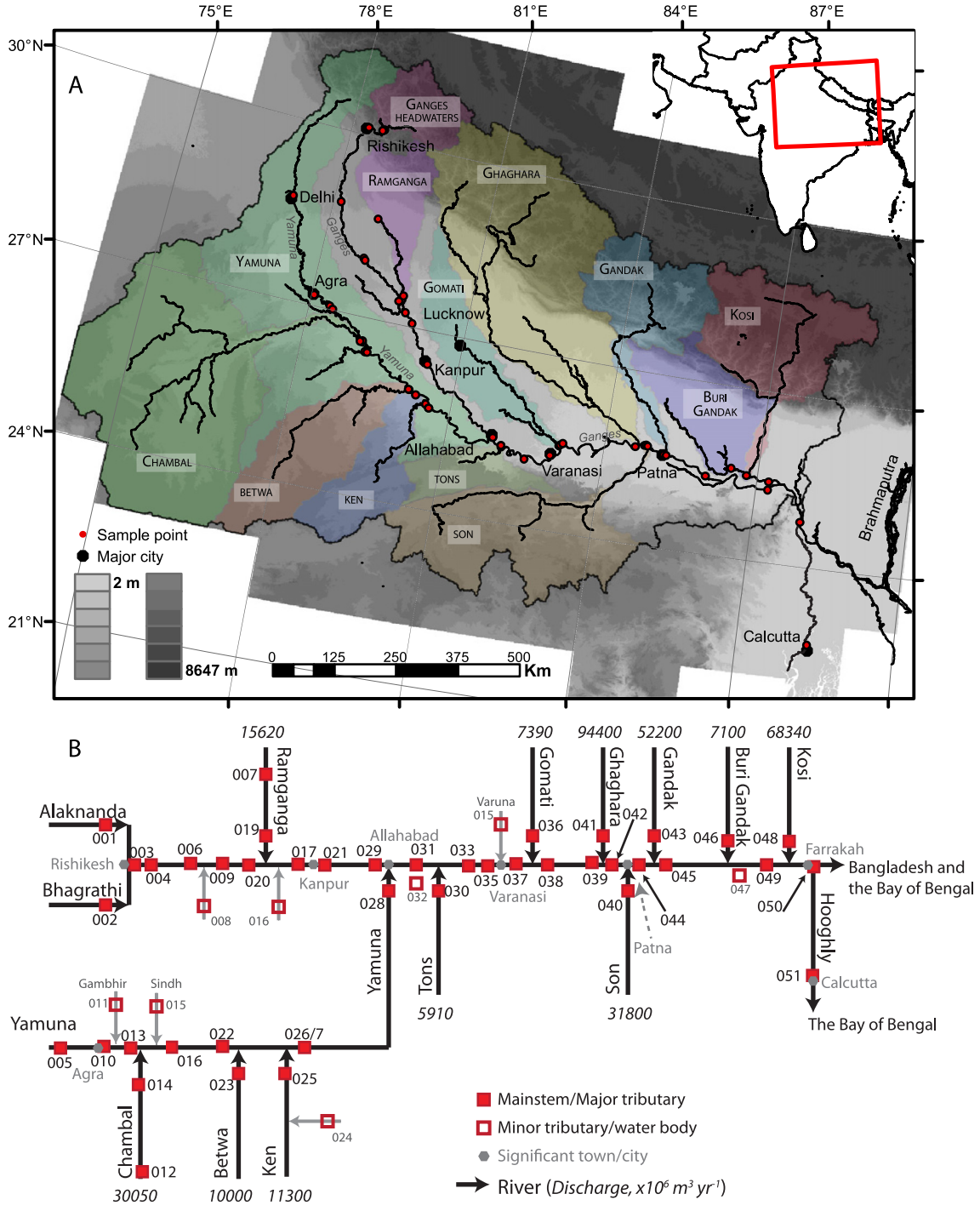

Fig. 1. Representations of the Ganges basin, including the major tributaries and sampling points. A: The major tributaries and their drainage basins, derived using GIS capabilities from SRTM topographic data (Jarvis et al., 2008). B: A schematic of the hydrographic network showing the location of samples on the major tributaries (filled red squares) and minor streams or water bodies (open red squares). For reference, large cities are indicated on both representations. The discharges of the major tributaries are given in italics in 10 $m^3\,yr^{-1}$. The uncoloured areas in panel A we assume are direct, unaccounted for, alluvial plain inputs to the Ganges. (For interpretation of the references to colour in this figure legend, the reader is referred to the web version of this article.)

from the base of the Himalaya at Rishikesh to the Hooghly distributary system at Calcutta (Fig. 1) and include all major tributaries of Himalayan, shield and GAP origin, plus several small streams directly draining the active floodplains. In some cases (the Yamuna, Ramganga and Chambal), tributaries were sampled at multiple distances from their confluence with the Ganges. The mainstem and a tributary were generally sampled independently just upstream of their confluence, and then approximately 20 km downstream to allow quantification of their mixing. Sampling occurred between the 10th and 28th September 2013, at the end of the annual flood pulse. The channel distance upstream of the mouth of the Hooghly in the Bay of Bengal and the catchment delineations were defined using a river network derived within the geographical information system (GIS) software ESRI ArcGIS 10.3 using the shuttle radar topography mission (SRTM) digital elevation model (DEM) at a 3 arc-second resolution (Fig. 1).

At each site, 5 L surface water (~0.25 m) samples were collected from a boat positioned near the quickest flowing water, or

directly from the bank or a bridge when no boat was available. When a boat was available, water was also collected at selected points in the water column with a ballasted 3-L Van Dorn horizontal water sampler (or, for the first seven sites, a ballasted 5-L polyethylene (PE) container). Samples were stored in 5-L pre-rinsed PE containers and filtered within a few hours of collection through 142 mm diameter, 0.4 µm pore-size polycarbonate membrane filters using a Teflon-coated pressure-filtration unit (MaxFil) at a maximum of $\sim 0.42 \times 10^6$ Pa (ca. 60 psi). A 100 ml sample from this filtration was retained in an HDPE bottle for analysis of major anions and silicon isotope composition (δ^{30}Si) of the dissolved Si. For the surface waters (and deeper waters, when taken), a subsample of 30 ml was filtered immediately after collection into HDPE bottles using a syringe and a 0.4 µm pore cartridge filter (Millipore Sterivex) and acidified by addition of ~50 µl of 65% w/w HNO_3 for the analysis of Si and major cations. All bottles were sealed with Parafilm and stored in the dark at ambient temperatures.

3.2. Major ion geochemistry

Major anions were measured by ion-chromatography at the Department of Biology, Lund University while Si and major cations were measured with a Varian 720 ICP-AES, at the Department of Geography, University College London, with estimated precision <5%.

3.3. Silicon isotope geochemistry

All isotope ratios are presented in delta notation (δ^{30}Si, in per mil), relative to the standard NBS28:

$$\delta \text{ (in ‰)} = \left[\frac{R_{sam} - R_{std}}{R_{std}} \right] \times 1000, \quad (1)$$

where R_{sam} and R_{std} are the ratios of the heavy (^{30}Si or ^{29}Si) to the light isotope (^{28}Si) in the sample and in NBS28, respectively.

Silicon isotope ratios of DSi were measured on a Thermo Finnigan Neptune MC-ICP-MS at the Pole Spectrométrie Océan (PSO, Ifremer, Brest). Sample purification followed a two-step procedure outlined in Frings et al. (2014). First, silicon was precipitated with triethylamine molybdate ("TEA-Moly") to form a triethylamine silicomolybdate complex, which was collected by filtration and combusted for 10 h at 1000 °C to form a nearly-pure SiO_2 polymorph (a mixture of cristobalite and tridymite) (De la Rocha et al., 1996). Second, this silica was dissolved in HF at an Si:F ratio of 1:100 before anion exchange column chemistry following Engström et al. (2005) to eliminate remaining contaminants. The silicon was eluted at 11.2 ppm in a 0.15 M HNO_3 and 5.5 mM HF matrix. Column yields were assessed colourmetrically with matrix-matched standards. The solution was diluted to 2 ppm Si with 2% nitric acid before doping to 0.1 ppm Mg for the mass-spectrometry. All acids were Merck Suprapur grade and all dilutions were made with MilliQ deionised distilled water (18.2 $M\Omega\,cm^{-1}$)

δ^{30}Si was assessed on the 2 ppm Si solution on the Neptune operating in dry-plasma mode with an Apex desolvating nebulizer for sample introduction. The Neptune was operating in medium resolution (resolving power, $m/\Delta m \approx 4000$), and samples were bracketed with precisely matrix-matched standards. Any individual measurements with sample beam intensities outside ±15% of the bracketing standards were rejected. Mg isotopes were measured simultaneously to monitor and correct for instrumental mass-bias following Cardinal et al. (2003). Internal measurement precisions are typically <0.1‰. A long-term precision (1σ SD), including column chemistry, was ±0.07‰, based on 29 separate analyses of an NBS28 preparation between July 2009 and November 2013.

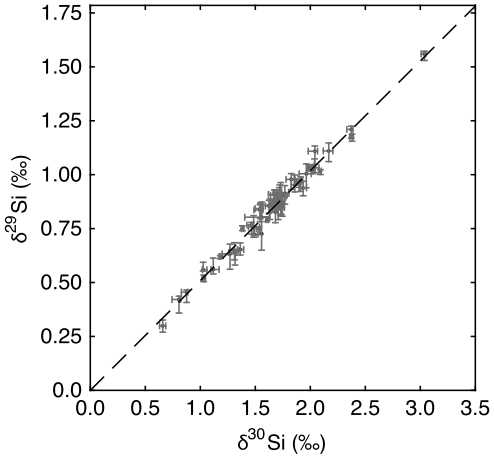

Fig. 2. Three-isotope plot (δ^{29}Si vs. δ^{30}Si) for all silicon isotope data points included in this manuscript. The calculated regression line ($\delta^{29}Si = 0.512\delta^{30}Si$; dashed line) is indistinguishable from a theoretical kinetic fractionation line ($\delta^{29}Si = 0.5092 \times \delta^{30}Si$), emphasising the successful removal of polyatomic interferences during mass spectrometry.

A conservative value of ±0.1‰ is used as the uncertainty estimate in this manuscript, unless the internal precision associated with an individual measurement is larger. All results plot on a mass-dependent fractionation line $\delta^{29}Si = 0.512 \times \delta^{30}Si$ in a three-isotope plot (Fig. 2), indistinguishable from the theoretical kinetic gradient, emphasising the successful removal of polyatomic interferences during measurement. Machine accuracy was assessed in a separate analytical session using the secondary standards Diatomite and Big-Batch prepared following the same protocols. These yielded values in agreement with the results from an inter-lab comparison (Reynolds et al., 2007), i.e. +1.20‰ vs. +1.26 ± 0.1‰ for Diatomite ($n = 3$) and −10.48‰ vs. −10.48 ± 0.27‰ for Big Batch ($n = 2$).

4. Results

4.1. Water geochemistry

Silicon and major ion concentrations and δ^{30}Si values are presented in Supplementary Table 1. Dissolved Si (DSi) concentrations in the Ganges range from 72 to 332 µM (Table 1; Fig. 3) with a mean of 135 µM, just below the global mean river water concentration of ca. 160 µM (Dürr et al., 2011). There is some longitudinal variation in the Ganges mainstem, with concentrations increasing from ~75 µM at the base of the Himalaya to a plateau of ~135 µM around the Allahabad–Varanasi region, before decreasing to ~80 µM at Calcutta (Fig. 3a), almost identical to that seen previously (e.g. Fontorbe et al., 2013). Downstream variation occurs relatively smoothly, with step changes at confluences. This pattern is not mirrored in the Yamuna mainstem, which exhibits relatively constant [DSi] of ~150 µM. Of the major tributaries, the eastern Himalayan tributaries (the Ghaghara, Gandak and Kosi) have similar DSi concentrations of ~90 µM, while the non-Deccan southern tributaries (the Ken, Son and Tons) are slightly elevated, at ~150 µM. The Ramganga, a partially Himalayan river that drains the Siwaliks only, has higher [DSi] (190 and 184 µM) that are closer to concentrations in samples from the rivers draining the Deccan traps (Chambal, Betwa; mean = 219 µM) and of small floodplain systems (variable, but up to >300 µM), perhaps reflecting that the majority of the Ramganga catchment lies within the GAP.

With a mean concentration of 1210 µM, Ca^{2+} is the dominant cation in all the streams sampled here. On average, Ca^{2+} is 64% of cations (by concentration), dropping below 50% only at four

Table 1
Measured concentrations of Si and other major elements in waters of the Ganges basin at the most downstream point of each respective system, and calculated fluxes (mass time^{-1}) and yields (mass area^{-1} time^{-1}) based on measured concentrations, derived areas (Fig. 1) and literature discharge values. Total yields are area weighted.

Subbasin	fQ[a] (–)	Concentration (observed) (μM)						Fluxes (Gmoles yr^{-1})						Yield (kmol km^{-2} yr^{-1})					
		Si	Mg	Ca	Na	K	Sr	Si	Mg	Ca	Na	K	Sr	Si	Mg	Ca	Na	K	Sr
Northern Himalayan																			
Ganges at Rishikesh	0.052	80	107	689	70	122	2.6	1.9	2.6	16.5	1.7	2.9	0.1	88	117	756	77	134	2.9
Ramganga	0.034	184	396	1982	423	295	13.8	2.9	6.2	31.0	6.6	4.6	0.2	108	231	1158	247	172	8.1
Ghaghara	0.206	85	200	1263	124	121	6.8	8.0	18.9	119.2	11.7	11.4	0.6	55	128	810	80	78	4.4
Gandak	0.114	72	173	1066	65	135	5.7	3.8	9.0	55.7	3.4	7.1	0.3	75	181	1116	68	141	6.0
Kosi	0.149	98	75	725	85	101	2.1	6.7	5.1	49.6	5.8	6.9	0.1	103	79	759	89	106	2.2
Yamuna at Him. Front	0.023	154	314	1663	636	195	17	1.7	3.4	17.9	6.8	2.1	0.2	172	351	1863	712	219	19.0
Yamuna and Tributaries																			
Yamuna at Allahabad	0.203	152	229	1417	570	128	17.4	14.1	21.3	131.8	53.0	11.9	1.6	35	53	329	132	30	4.0
Chambal	0.065	208	295	1168	529	96	20.7	6.2	8.9	35.1	15.9	2.9	0.6	39	56	220	100	18	3.9
Betwa	0.022	215	233	1341	503	76	16.1	2.2	2.3	13.4	5.0	0.8	0.2	41	45	257	96	15	3.1
Ken	0.025	192	200	1418	350	56	13.2	2.2	2.3	16.0	4.0	0.6	0.2	64	67	474	117	18	4.4
Unaccounted for[b]	0.067	152	269	1379	602	168	16	4.7	8.3	42.6	18.6	5.2	0.5	32	57	292	128	36	3.4
Southern Peninsular																			
Tons	0.013	110	167	1216	232	66	12.4	0.7	1.0	7.2	1.4	0.4	0.1	32	49	356	68	19	3.6
Son	0.069	157	121	801	201	56	4.6	5.0	3.9	25.5	6.4	1.8	0.2	65	50	332	83	23	1.9
Alluvial Plain																			
Gomati	0.016	111	316	1186	542	136	12.2	0.8	2.3	8.8	4.0	1.0	0.1	23	65	245	112	28	2.5
Buri Gandak	0.015	131	163	1508	188	135	7.3	0.9	1.2	10.7	1.3	1.0	0.1	22	28	255	32	23	1.2
Unaccounted for[b]	0.129	152	269	1379	602	168	16	9.0	16.0	81.9	35.7	10.0	1.0	85	151	773	337	94	9.0
Weighted averages																			
Estimated at Farrakah		*123*	*199*	*1156*	*280*	*128*	*9*												
Observed at Farrakah		*98*	*145*	*1068*	*186*	*123*	*7*												
Discrepancy (%)		*21*	*27*	*8*	*33*	*4*	*25*												
Total fluxes and yields[c]																			
Himalayan rivers								24.9	45.2	289.7	36.0	35.0	1.5	82	140	915	115	114	5
Southern Peninsular								16.2	18.3	97.2	32.6	6.5	1.1	32	59	303	125	36	3
Alluvial Plain								15.5	27.8	144.0	59.7	17.1	1.6	51	53	305	93	20	3

[a] fQ = fraction of total discharge at Farrakah, based on compilation in Jain et al. (2007). fQ sums to more than unity because the Yamuna tributaries are included twice; this has been accounted for in the flux and yield calculations. Unaccounted for discharge refers to the fraction of discharge for a given point on the mainstem or Yamuna that is in excess of the sum of all the upstream tributaries with available discharge data, and is assumed to derive from the areas not part of one of the tributaries as defined in Fig. 1.

[b] Major element geochemistry taken as mean of alluvial plain water samples (supplementary Table 1).

[c] Himalayan rivers are defined as the sum of Yamuna at Delhi, Ganges at Rishikesh, and Ramganga, Ghaghara, Gandak and Kosi at their confluence with the Ganges, which implicitly blurs the distinction between Himalaya and GAP. Southern Peninsular rivers are the sum of the Chambal, Betwa, Ken, Tons and Son and Alluvial Plain rivers are the sum of the Gomati and Buri Gandak, plus the discharge at Farrakah unaccounted for by the above rivers.

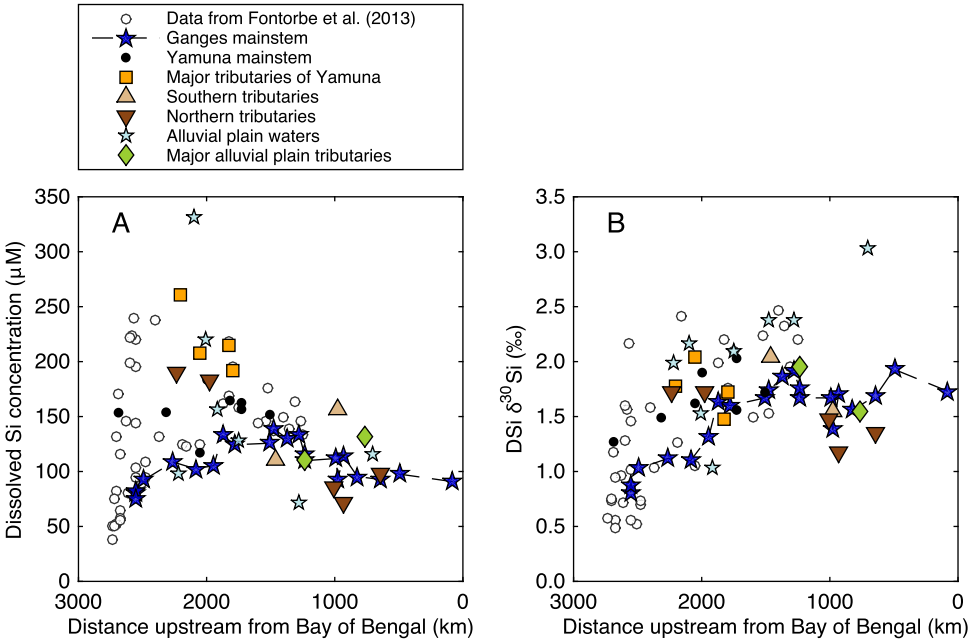

Fig. 3. Downstream variation in A: dissolved Si (DSi) concentrations (μM) and B: silicon isotopic composition (δ^{30}Si) of DSi in the Ganges basin. Data from Fontorbe et al. (2013), collected mostly in mountain streams and the alluvial Gomati River, are shown for comparison.

sites. The first three of these sites correspond to closely spaced samples with unusually elevated [Na] (~1500 µM) along the Yamuna and the fourth to the Varuna, a small, highly polluted stream draining the alluvial plain before its confluence with the Ganges at Varanasi. Bicarbonate (HCO_3^-) is the dominant anion, with an average (calculated) concentration of 2420 µM. The next most dominant anion after bicarbonate is Cl^- with a mean concentration, after rainwater-correction (see below) of 500 µM. Some extremely high Cl^- concentrations in excess of Na (>4000 µM Cl) occur in several Yamuna mainstem samples.

4.1.1. Solute mass balance

Taking discharges for the major rivers from Kothyari and Garde (1991) and assuming our measured concentrations are representative, and that the relative discharges between tributaries are constant, the solute budgets of the major elements (i.e. Si, Mg, Ca, Na, K and Sr) broadly balance in the Ganges basin (Table 1), with the concentrations at the lowermost sample (sample 051; Farrakah Barrage, near the Bangladeshi border) tending to lie a little below the weighted sum of the upstream inputs. Calculated fluxes (kmol yr^{-1}) and yields (Gmol $km^{-2}\,yr^{-1}$) emphasise the importance of the solutes of Himalayan origin at Farrakah. The majority of Ca, Mg and K derive from the Himalaya, while Si derives in a roughly 50/50 ratio from the Himalaya and the rest of the catchment. Na and Sr originate predominantly from non-Himalayan areas.

Dissolved Si yields in the Ganges range from a mean of 100 kmol $km^{-2}\,yr^{-1}$ in the Himalayan rivers to 48 and 41 kmol $km^{-2}\,yr^{-1}$ in the peninsular and alluvial plain rivers, respectively (Table 1). These values cluster around the global mean DSi yield of c. 55 kmol $km^{-2}\,yr^{-1}$ (3.3 t $km^{-2}\,yr^{-1}$; Dürr et al., 2011), and are in good agreement with previous work in the Gomati and Son rivers (Rai et al., 2010).

4.2. Silicon isotope geochemistry

All DSi samples, with δ^{30}Si ranging from +0.81‰ to +3.04‰ (Fig. 5a), are enriched in ^{30}Si relative to silicate rocks (δ^{30}Si of mean upper continental crust (UCC) = −0.25 ± 0.16‰, Savage et al., 2013). Samples from the Ganges mainstem increase from <+1‰ at base of the Himalaya to a relatively constant value of ~+1.7‰ after ca. 500 km. This downstream increase is consistent with δ^{30}Si of DSi in the Chiangjiang and Huang He (the Yangtze and Yellow Rivers), two other large rivers draining the Himalayan–Tibetan plateau (Ding et al., 2004, 2011). Smaller rivers draining the GAP have generally higher δ^{30}Si (mean = 2‰) (Fig. 3b). Taking the samples as a whole, there is no clear relationship with [DSi] (Fig. 4) and the points fall within a roughly triangular array, and well within the range previously observed in river waters worldwide of −0.14‰ to 4.66‰ (mean = 1.38‰, $n = 528$) (Frings, 2014).

The major southern tributaries (the Chambal, Betwa, Ken, Son and Tons) have similar δ^{30}Si values, falling between +1.48‰ and +2.04‰ while the major northern tributaries draining the Himalaya (the Ramganga, Ghaghara, Gandak and Kosi) have slightly lower δ^{30}Si (+1.18 to +1.73‰). The highest but most variable δ^{30}Si occurs in the small streams draining the alluvial plain directly: +1.03 to +2.38‰ in the Ganges subbasin and +1.53 to +2.09‰ in the Yamuna/Chambal subbasins. The highest measured value of +3.04‰ derives from an inundated region in the active floodplain, hydrologically isolated from the main channel. This high DSi, high δ^{30}Si value is problematic to explain but may relate to a high degree of evaporation in concert with high biogenic silica production, as seen in e.g. the Nile river (Cockerton et al., 2013). River elemental concentrations and δ^{30}Si value after a confluence are generally within error of the discharge-weighted sum of the two joining streams, arguing against large in-stream processes impacting the solute geochemistry. One exception may be the penultimate sample, (#050), collected immediately downstream of the Farrakah Barrage, which is slightly higher than the two nearest upstream samples – the Kosi River and the Ganges upstream of its confluence with the Kosi (Fig. 1; Supplementary Table 1). This may be due to conversion of river DSi to diatom silica in the less turbid waters behind the barrage, though this is speculative.

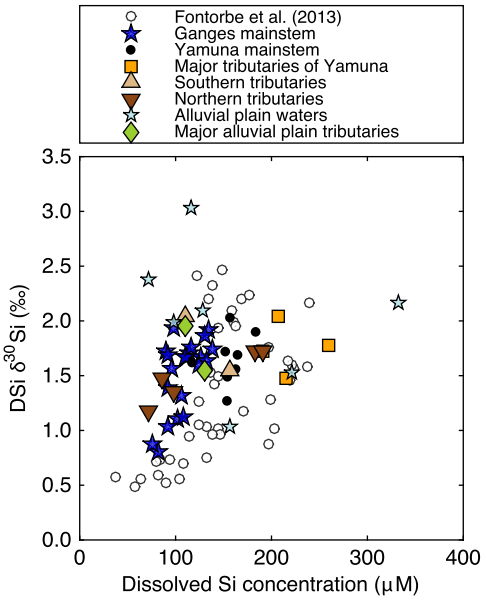

Fig. 4. Silicon isotope composition (δ^{30}Si) vs. dissolved Si concentrations (µM) in Ganges basin river waters.

5. Discussion

We can conceptualise silicate weathering fluxes as the sum of two processes: the initial breakdown at the solid–solution interface, and the formation of secondary (alumino-)silicates – i.e. clays and related minerals – that removes some fraction of the new solutes. The ratio of primary mineral breakdown to secondary mineral formation can be seen as an index of weathering congruency (Pogge von Strandmann and Henderson, 2014). Congruent weathering produces solutes with elemental stoichiometries and isotopic compositions close to the parent material (i.e. lower δ^{30}Si), whereas incongruent weathering causes the composition of the solutes to deviate from that of the parent material (i.e. higher δ^{30}Si, as more Si is stored in clays). The use of DSi fluxes in the calculation of weathering mass-budgets has been limited to date because the incorporation of mobilised Si into secondary minerals or biogenic silica – i.e. the degree of weathering congruency – is hard to account for. In the following, we suggest the δ^{30}Si value of river DSi primarily reflects weathering congruency, and can therefore be used to correct observed Si yields and derive initial silicate-weathering rates.

5.1. Riverine behaviour of silicon isotopes

Consideration of published river silicon isotope data supports the interpretation that a primary driver is weathering congruency. Unweathered silicates at the Earths surface define a relatively constrained range of δ^{30}Si – a compilation of rock δ^{30}Si values, weighted by abundance, yields a global upper continental crust (UCC) value of −0.25 ± 0.16‰ (Savage et al., 2013), and conservation of mass requires that there can be no net isotopic fractionation during their dissolution (Ziegler et al., 2005),

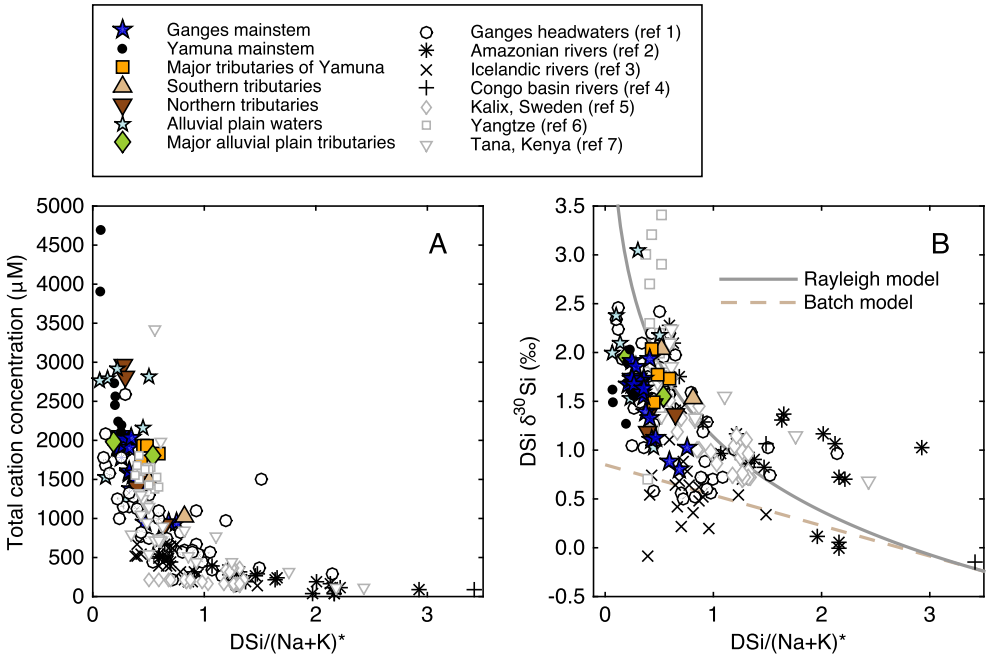

Fig. 5. Si is increasingly removed from solution at higher solute concentrations, which imparts a greater observable fractionation. A: Increasing retention of Si into secondary phases (i.e. decreasing Si/(Na + K)*, where (Na + K)* indicates the sum of Na and K concentrations corrected for cyclic inputs; see main text for details) at increasing solute (total cation) concentrations. B: Increasing fractionation relative to bedrock with increasing Si retention (decreasing Si/(Na + K)*). Panel B also shows expected evolutions of δ^{30}Si as DSi as it is progressively removed relative to (Na + K), for a Rayleigh model (solid grey line) and a steady-state model (dashed brown line), assuming an initial solution with δ^{30}Si = −0.25‰ and Si/(Na + K) of 3.53 (Hughes et al., 2013). A range of river waters worldwide are plotted for comparison in both panels. Element concentrations have only been corrected for rainfall inputs if performed in the original publication. References: 1 – Fontorbe et al. (2013), 2 – Hughes et al. (2013), 3 – Georg et al. (2007), 4 – Cardinal et al. (2010), 5 – Engström et al. (2010), 6 – Ding et al. (2004), 7 – Hughes et al. (2012). (For interpretation of the references to colour in this figure legend, the reader is referred to the web version of this article.)

so variability in source rock δ^{30}Si is unlikely to impart significant variability to the δ^{30}Si of the initial solution, especially at large spatial scales. There are then two remaining pathways to altering a δ^{30}Si value of DSi. The first is to create new solid phases, either abiotically (e.g. clay precipitation from a saturated solution) or biologically (e.g. diatom growth or plant phytolith production). These processes consistently discriminate against the heavy ^{30}Si isotope, creating lower δ^{30}Si products and leaving the residual solution with higher δ^{30}Si (De la Rocha et al., 1997; Oelze et al., 2014; Opfergelt et al., 2010; Ziegler et al., 2005). The second pathway is to add new DSi through the dissolution of isotopically distinct secondary minerals (including biogenic silica).

Since at steady-state, over an annual cycle, any dissolution of a secondary phase must be balanced by its prior production, the second pathway is unlikely to have a major effect at large scale, though small scale or transient impacts are plausible. A number of observations worldwide suggest that removal from solution (i.e. pathway 1) is the most important mechanism in determining river δ^{30}Si. The samples with the lowest values yet measured (c. 0.0‰ to −0.1‰) derive from locations that exhibit near-congruent primary mineral dissolution. These include 'blackwater' rivers in tropical environments (Cardinal et al., 2010; Frings, 2014; Hughes et al., 2013), but also some glacial rivers in Iceland (Georg et al., 2007). Correspondingly, of all reported measurements, the highest δ^{30}Si values come from systems where a high degree of Si removal into clays or biogenic silica is expected. These include the semi-arid Nile basin (Cockerton et al., 2013) and the highly agricultural Yangtze river (Ding et al., 2004), where δ^{30}Si reaches +4.7‰ and +3.4‰, respectively. For rivers with δ^{30}Si monitored over an annual cycle, there is a tendency for the highest δ^{30}Si values to coincide with the periods of lowest discharge and DSi export (Delvaux et al., 2013; Engström et al., 2010; Georg et al., 2006; Hughes et al., 2011, 2013; Pokrovsky et al., 2013). This is observed in Ganges basin itself: dry-season water samples from several rivers presented by Georg et al. (2009) are consistently offset to higher values than those we have measured on the same or nearby rivers. This implies that at greater mean water residence times, clay mineral formation (or biogenic silica production) is increased, pushing the δ^{30}Si of residual DSi higher. A similar observation can be made based on changes in δ^{30}Si along river longitudinal transects (Cardinal et al., 2010; Cockerton et al., 2013; Ding et al., 2004, 2011; Fontorbe et al., 2013; Hughes et al., 2012): as with the data presented here, there is a tendency for δ^{30}Si to increase downstream as water and sediment residence times increase. Again, the greater interaction times implied should increase the degree of clay formation as the limits to clay precipitation (and therefore Si isotope fractionation) are more likely to be overcome, whether these limitations are primarily kinetic, thermodynamic, or a mixture. Pogge von Strandmann and Henderson (2014) reach a similar conclusion with respect to lithium isotopes, based on a negative relationship between the isotopic composition of dissolved lithium (δ^{7}Li) and uplift rates in the New Zealand Alps.

5.2. Silicon geochemistry in the Ganges alluvial plain: first order controls and potential for use as a weathering index

Overall, the behaviour of silicon in the Ganges basin corroborates the above. At lower solute concentrations, silicate weathering generally becomes more congruent, i.e. more stoichiometric conversion of the available minerals to solutes. Conversely, at higher solute concentrations, the fraction of Si incorporated into secondary phases becomes larger. To a first degree, this is seen in a plot of total cations against DSi/(Na + K)* (Fig. 5a, where the asterisk denotes values corrected for rainfall solute inputs following Galy and France-Lanord, 1999 using a larger rainwater chemistry database included in the supplementary online material). Na and K are hosted predominantly in silicates, so higher DSi/(Na + K)*

(i.e. approaching source material) reflects more congruent weathering, whereas lower values reflect greater relative retention (as clays or biogenic silica) of the DSi released from dissolution of primary minerals. DSi/(Na + K)* ranges between 0.05 and 0.8, consistent with previous work in the Ganges basin (Sarin et al., 1989), but unfortunately a number of caveats to the use of (Na + K)* for normalisation preclude using this as a quantitative index of weathering congruency (cf. Hughes et al., 2013). These include i) imprecisely known bedrock Si/(Na + K) ratios (and whether or not to include the very slowly reactive quartz component), ii) the incorporation of K into secondary phases, though this is likely small in comparison to its mobilisation from the K-rich Himalayan bedrock, iii) other, non-silicate inputs of Na or K from e.g. soil-salts.

Incorporation of silicon into secondary solids by either biogenic or abiotic means imparts a silicon isotope fractionation (e.g. Oelze et al., 2014; Opfergelt et al., 2006). Correspondingly, δ^{30}Si increases with decreasing DSi/(Na + K)* (Fig. 5b), both in the Ganges and in a range of global rivers. In other words, the greater the fraction of Si retained into secondary minerals (or biogenic silica), the greater the observed deviation from a typical primary mineral value ($\sim -0.25‰$; Savage et al., 2013). This is consistent with previous Si isotope work in the Ganges basin (Fontorbe et al., 2013) which also inferred that weathering became less congruent at higher solute concentrations.

Although the dominant mechanism of DSi removal from solution is likely incorporation into neoformed clay minerals, one potentially important anthropogenically induced DSi removal mechanism may be the retention of biogenic silica remains in reservoir sediments (Frings et al., 2014), with an associated biological fractionation. However, the Ganges basin is not yet excessively dammed. The Global Reservoir and Dam (GRanD) database lists 80 reservoirs within the Ganges basin, of which only three have a surface area greater than 100 km^2 (Lehner et al., 2011). The total area of natural lakes and wetlands is larger (Lehner and Doll, 2004), so any net 'natural' biogenic silica sequestration here is likely more important. The construction of large diversionary irrigation canals (Jain et al., 2007) may similarly have increased the potential for enhanced production of biogenic silica. Note that even if biological activity is the main mechanism by which DSi is removed from solution relative to Na and K, the impact on δ^{30}Si of the residual DSi will be very similar, and our attempt below to quantify this removal is independent of the actual DSi sink.

5.2.1. A weathering index based on silicon isotope geochemistry

Experimental and theoretical evidence suggests the range of δ^{30}Si observed in nature can be mostly attributed to unidirectional kinetic isotope effects (Dupuis et al., 2015; Oelze et al., 2014), i.e. there is little evidence for equilibrium isotope fractionation between low temperature precipitates (including clays) and solutions (which should tend to leave the clays isotopically heavier). Given this kinetic dominance (i.e. mostly forward reactions), two simple conceptual models are commonly applied to the evolution of the isotopic composition of a given mass of DSi as it is removed from solution. Firstly, in a system that is closed with respect to further DSi inputs and the product has no further interactions, the δ^{30}Si of the residual DSi follows a Rayleigh distillation curve:

$$\delta^{30}\mathrm{Si}_{\mathrm{residual}} = \delta^{30}\mathrm{Si}_{\mathrm{initial}} + {}^{30}\varepsilon_{\mathrm{removal}} \cdot \ln(f) \quad (2)$$

Where $\delta^{30}\mathrm{Si}_{\mathrm{residual}}$ is the isotopic composition of DSi after a fraction f has been removed with a per mil enrichment, ${}^{30}\varepsilon_{\mathrm{removal}}$, from DSi with an initial isotopic composition $\delta^{30}\mathrm{Si}_{\mathrm{initial}}$. Rearranging to find f:

$$f = e^{(\Delta\delta^{30}\mathrm{Si}/{}^{30}\varepsilon_{\mathrm{removal}})} \quad (3)$$

where $\Delta\delta^{30}$Si is the difference between the δ^{30}Si of the initial and residual DSi. We will refer to this as a Rayleigh model. Alternatively, the DSi can exist in an open system, such that it constantly receives 'fresh' DSi (e.g. from primary mineral weathering). If a dynamic equilibrium is reached such that removal into secondary phases balances the supply of new DSi (Reynolds et al., 2006), the isotopic composition of the residual water:

$$\delta^{30}\mathrm{Si}_{\mathrm{residual}} = \delta^{30}\mathrm{Si}_{\mathrm{initial}} - {}^{30}\varepsilon_{\mathrm{removal}}(1 - f) \quad (4)$$

where f is:

$$f = 1 - (\Delta\delta^{30}\mathrm{Si}/{}^{30}\varepsilon_{\mathrm{removal}}) \quad (5)$$

This is sometimes referred to as a 'steady-state' or 'batch equilibrium' model (Bouchez et al., 2013; Georg et al., 2007; Hughes et al., 2013), since the evolution of isotopic composition as a function of f is the same as for a reversible reaction at equilibrium in a closed system; we will refer to it as a batch model. In the case that the supply of new DSi is large relative to the removal, $f \approx 1$, $\delta^{30}\mathrm{Si}_{\mathrm{residual}} \approx \delta^{30}\mathrm{Si}_{\mathrm{initial}}$ and the product is simply $\delta^{30}\mathrm{Si}_{\mathrm{initial}} + {}^{30}\varepsilon_{\mathrm{removal}}$. In both models, there are two unknowns: $\delta^{30}\mathrm{Si}_{\mathrm{initial}}$ and ${}^{30}\varepsilon_{\mathrm{removal}}$, the per mil fractionation associated with DSi removal from solution. For the large-scale, mixed lithologies of the Ganges subbasins, a mean UCC δ^{30}Si of $-0.25‰$ (Savage et al., 2013) can satisfactorily approximate the δ^{30}Si of the DSi initially released from primary minerals (discounting any net fractionation during dissolution). Because the DSi in any given sample reflects the integration of a number of different flowpaths of water that have experienced different histories, a single, lumped fractionation is also reasonable, and has been applied successfully at a range of scales (Bouchez et al., 2013). ${}^{30}\varepsilon_{\mathrm{removal}}$ is therefore an integrative function of all DSi-consuming reactions that is likely in the region of $-1.50‰$ based on compiled values for both biological and abiotic processes (Opfergelt and Delmelle, 2012), and in line with recent experimental work (Oelze et al., 2014).

A choice needs to be made between the two isotope evolution models. Some evidence suggests application of the batch fractionation model, as used by e.g. Bouchez et al. (2013) is inappropriate here, since the greatest allowable fractionation of DSi relative to the parent material under an open-system model with ${}^{30}\varepsilon_{\mathrm{removal}} = -1.50‰$ is $+1.25‰$, which is often exceeded, both in the Ganges and elsewhere. We could therefore argue that isotope fractionation for a given flowpath is dominantly driven by Rayleigh style fractionation. Fig. 5b shows the isotope evolution as a function of DSi/(Na + K)* as predicted by the two models. Visually, the Rayleigh model seems to capture the overall behaviour of global rivers. However, work on silicon isotope systematics in Amazonian and Icelandic streams (Georg et al., 2007; Hughes et al., 2013) and lithium isotopes, again in the Amazon (Dellinger et al., 2015) suggests some individual rivers have a tendency to plot along a line defined by the batch model, whilst other rivers will follow the Rayleigh pathway. A more quantitative index of f is needed to discriminate between the two. Further, both models (Rayleigh or batch) strictly apply to the evolution of isotopic compositions in a simple, discrete package of DSi. We overcome this limitation by conceptualising the DSi in any given river sample as resulting from the summation of many small flowpaths, each contributing a fraction of the total, and with its own isotopic evolution.

Interestingly, in the case of systems following the Rayleigh model, because of the mixing of multiple flowpaths, one cannot simply apply equation (3) to a river δ^{30}Si value and obtain an accurate estimate of f, our proposed index of silica-weathering congruency. The mixing of multiple flowpaths imposes the problem that f as calculated from equation (3) will not necessarily correspond to the f_{true}, the 'true' fraction remaining in solution.

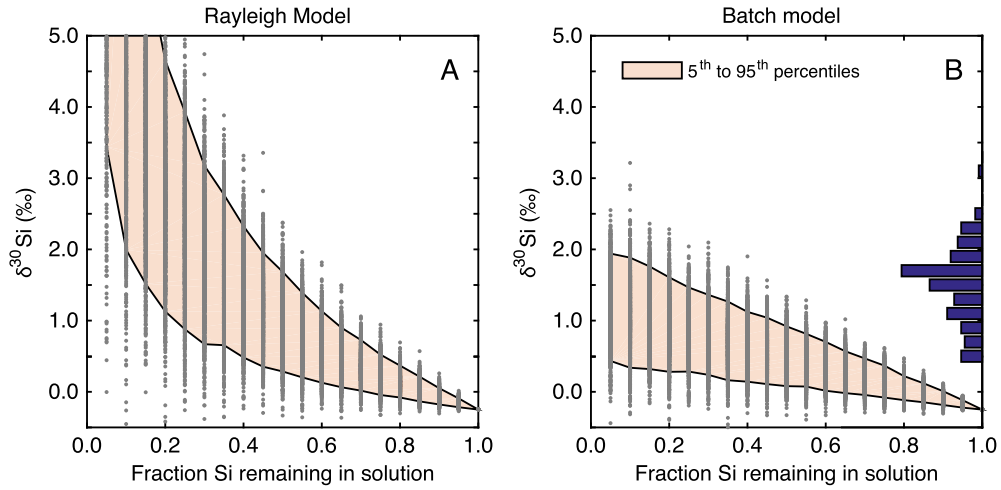

Fig. 6. Simulation of possible ranges of δ^{30}Si for a given f_{Si}, for A: a Rayleigh-style system and B: a steady-state system. In both cases, the δ^{30}Si–f_{Si} calibration is derived using 1500 iterations (grey dots) per step in f_{Si} and using values of −0.25‰ for $\delta^{30}Si_{initial}$ and -1.5 ± 0.5‰ for $^{30}\varepsilon_{removal}$ (see main text for details). The shaded areas represent the 5th to 95th percentile of simulated data, while the histogram on the y-axis of panel B displays the relative frequency of measured river DSi δ^{30}Si in the Ganges basin at 0.2‰ bin intervals, including data from Fontorbe et al. (2013) and Georg et al. (2009). These models can be seen as sensitivity.

This is because the observed δ^{30}Si is the flux-weighted average of the individual flowpath δ^{30}Si values, which themselves are a non-linear function of the individual flowpath's f values (cf. equation (2)):

$$\delta^{30}Si_{obs} = \sum X_i \cdot \left[\delta^{30}Si_{initial} + {}^{30}\varepsilon_{removal,i} \cdot \ln(f_i)\right] \quad (6)$$

for i flowpaths contributing a fraction X_i of the total Si. Conversely, f_{true} is simply the (linear) weighted average of the individual f values:

$$f_{true} = \sum X_i \cdot f_i \quad (7)$$

This imposes the constraint that, for systems that experience Rayleigh fractionation, f inferred from a measured δ^{30}Si value via equation (3) will be less than f_{true}.

To account for the departure from ideal behaviour caused by mixing of multiple flowpaths and to propagate the uncertainties associated with imprecisely known fractionations, we performed Monte-Carlo style simulations to derive the expected range of δ^{30}Si values in river water DSi for any given f_{true} (Fig. 6). We achieve this using artificially generated data with n flowpaths, where each flowpath i is randomly assigned (i) a fraction of the total flux (X_i), (ii) a per mil solid–solution enrichment factor, ($^{30}\varepsilon_i$) and (iii) a fraction remaining (f_i, from 0 to 1). X_i follows an exponential distribution, to account for the concept that some flowpaths will be more important than others. For each iteration, a lumped fractionation factor is randomly assigned, normally distributed around a mean of −1.50‰ with a standard deviation of 0.5‰. Within that iteration, the individual flowpath $^{30}\varepsilon_i$ values are further distributed around that lumped value, again with standard deviation = 0.50‰. Note that this is a conservatively large error estimate, and that our simple approach doesn't account for any correlation between these variables. Preliminary investigation showed the approach is insensitive to the number of flowpaths included above $n \approx 15$ so in the following all simulations take place with $n = 100$. These simulations are repeated twice, for the Rayleigh and batch fractionation models.

By varying the mean of the fraction remaining in solution, we obtain the range of δ^{30}Si values for a corresponding mean f_{true}. We achieve this by prescribing f_i to follow a beta distribution (i.e. constrained between 0 and 1) with mean = f_{true}. Fig. 6 shows the output of the simulations for $^{30}\varepsilon_{removal} = -1.50‰ \pm 0.50‰$ and $\delta^{30}Si_{initial} = -0.25‰$. The lower and upper limits of the range

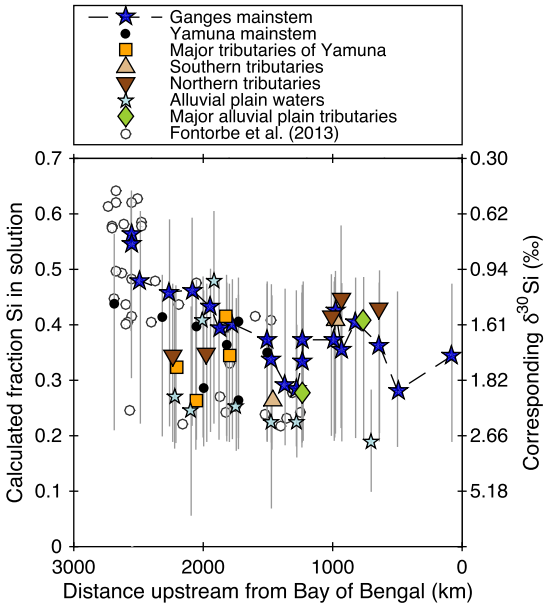

Fig. 7. The congruency of weathering with respect to Si, assuming Rayleigh style behaviour. Weathering congruency decreases with distance downstream, i.e. the fraction of initially solubilised Si remaining in solution decreases (alternatively: the fraction incorporated into clays/biogenic silica increases). The corresponding δ^{30}Si value for a given f_{Si} is shown on the right-hand axis; note that this scale is derived from the calibrated δ^{30}Si/f_{Si} relationship in Fig. 5a and is not linear. Uncertainties represent the 5th and 95th percentiles of the calibrated data.

of δ^{30}Si produced for a given f_{true} is taken as the 5th and 95th percentiles of 1500 individual iterations (the shaded envelopes in Figs. 6a and 6b) and includes both the uncertainty associated with imprecise knowledge of the true fractionation factor and the departure from ideal Rayleigh behaviour caused by mixing of multiple flowpaths (for the Rayleigh model only). Calibrating the observed δ^{30}Si against the mean of the simulations and these limits, f values in the Ganges basin fall between 0.54 (+0.14/−0.26) and 0.19 (+0.13/−0.13) (Fig. 7) if the rivers follow a Rayleigh model, or between 0 (i.e. near-total removal) and 0.46 if the batch model better describes their behaviour. The batch model produces results that are difficult to meaningfully interpret; all samples could imply near-total removal of Si from solution if the mean fractionation is towards the lower end of estimates. Conversely, even at the greater

Table 2
Summary of measured DSi yields and calculated initial mobilisation rates in the subbasins and the three domains of the Ganges basin (Himalaya, Plain, Southern Peninsula).

River	Observed			Rayleigh model			Batch model	
	Q[a] $\times 10^6$ ($m^3\ yr^{-1}$)	DSi yield[b] ($kmol\ km^{-2}\ yr^{-1}$)	$\delta^{30}Si$ ‰ ± 1sd	f[c] (5th to 95th percentile)	'Initial' DSi yield ($kmol\ km^{-2}\ yr^{-1}$)		f[c] (–)	'Initial' DSi yield ($kmol\ km^{-2}\ yr^{-1}$)
Himalayan Tributaries								
Ganges at Rishikesh	23 900	87	1.03 ± 0.10	0.48 + 0.15/−0.26	183 + 211/−42		<0.46	>189
Ramganga	15 620	107	1.72 ± 0.10	0.34 + 0.16/−0.21	317 + 516/−99		< 0.16	>676
Ghaghara	94 400	54	1.47 ± 0.10	0.39 + 0.15/−0.23	142 + 212/−39		<0.26	>206
Gandak	52 200	75	1.18 ± 0.10	0.44 + 0.15/−0.25	170 + 215/−42		<0.39	>192
Kosi	68 340	102	1.36 ± 0.10	0.41 + 0.14/−0.24	253 + 351/−66		<0.30	>342
Yamuna at HF	10 750	172	1.27 ± 0.10	0.43 + 0.14/−0.24	125 + 165/−32		<0.35	>499
Yamuna and Tributaries								
Yamuna at Allahabad	93 020	35	1.72 ± 0.10	0.34 + 0.16/−0.21	104 + 169/−33		< 0.16	>222
Chambal	30 050	39	2.04 ± 0.10	0.29 + 0.15/−0.19	134 + 256/−46		< 0.05	>1001
Betwa	10 000	41	1.48 ± 0.10	0.38 + 0.15/−0.23	108 + 162/−30		<0.26	>159
Ken	11 300	64	1.73 ± 0.10	0.34 + 0.15/−0.21	189 + 307/−59		<0.16	>411
Unaccounted for[d]	30 920	36	2.00 ± 0.10[e]	0.29 + 0.15/−0.19	110 + 180/−35		<0.05	>620
Southern Tributaries								
Tons	5910	32	2.04 ± 0.10	0.29 + 0.15/−0.19	111 + 211/−38		<0.04	>825
Son	31 800	65	1.54 ± 0.10	0.37 + 0.15/−0.23	175 + 270/−51		<0.24	>276
Alluvial Plain								
Gomati	7390	22	1.96 ± 0.10	0.3 + 0.15/−0.20	76 + 138/−25		<0.07	>347
Buri Gandak	7100	22	1.55 ± 0.10	0.37 + 0.15/−0.22	60 + 93/−17		<0.23	>96
Unaccounted for[d]	26 476	38	2.00 ± 0.10[e]	0.29 + 0.15/−0.19	113 + 186/−36		<0.05	>731
Ganges at Farrakah								
Farrakah Barage	459 040	51	1.93 ± 0.10	0.31 + 0.15/−0.20	170 + 303/−56		<0.08	>1077
Discharge weighted means						*Si mobilisation rate* ($Gmol\ yr^{-1}$)[f]		
Himalayan		82	1.35	0.41	200	33.3	<0.31	>277
Alluvial Plain		32	1.95	0.30	107	54.5	<0.07	>581
Peninsular		51	1.76	0.34	150	45.6	<0.15	>561

[a] From Jain et al. (2007).
[b] From Table 1.
[c] Calculated as described in main text and Fig. 5, where $\delta^{30}Si_{initial} = -0.25$‰ and mean $^{30}\varepsilon_{removal} = -1.50 \pm 0.50$‰.
[d] As in Table 1.
[e] $\delta^{30}Si$ of 2.00‰ from average of alluvial plain waters (see supplementary Table 1).
[f] Assuming the Himalaya = 17%, peninsular India = 31% and the alluvial plain = 52% of the total catchment (0.98×10^6 km^2) (see Section 2).

end of fractionation estimates ($^{30}\varepsilon_{removal} < -2$‰), some samples do not overlap with the produced calibration, as shown by the $\delta^{30}Si$-histogram in Fig. 6b. We therefore focus here primarily on the results from the Rayleigh model, but suggest that in the future, approaches that combine the two models with an index of flowpath isolation could improve our understanding.

The $\delta^{30}Si$ values interpreted using a Rayleigh model indicate between 46% and 81% of Si released during weathering is retained in secondary phases (either aluminosilicates or biogenic silica; their formation is isotopically indistinguishable). In general, these values are comparable to values derived in Iceland, the Amazon and the Orinoco, using elemental stoichiometries (Georg et al., 2007; Hughes et al., 2013; Murnane and Stallard, 1990). Although the estimated uncertainties generally considerably overlap (Fig. 7), these are largely systematic in that they reflect our imprecise knowledge of the fractionating factors and processes associated with DSi removal from solution. It is therefore still possible to meaningfully interpret the overall trend shown in Fig. 7.

The Himalayan rivers (i.e. the Ganges headwaters, Ghaghara, Gandak and Kosi) have the greatest weathering congruency (~45% DSi remains in solution), and become progressively more incongruent (i.e. a greater proportion of Si retained in secondary minerals plus biogenic silica) with increasing distance from the Himalayan front (Table 2 and Fig. 7). Some small Himalayan catchments reported by Fontorbe et al. (2013) have f as high as 0.65 (+0.11/−0.26) ($\delta^{30}Si = 0.49$‰), while all their alluvial plain samples have $f < 0.48$ (Fig. 7). Here, the GAP and southern tributaries have similar weathering congruencies, with a mean of about 30% of initially mobilised DSi remaining in solution. We also note that the large Himalaya rivers (the Ghaghara, Gandak and Kosi; Fig. 1), at the point of sampling, have large portions, sometimes majorities, of their catchments in the GAP, blurring the distinction between mountain and lowland regions: samples from these rivers at the Himalayan Front would be beneficial but are not available. Our data show that Himalayan catchments weather more congruently, regardless of the fractionation model chosen. This is counter to a conventional interpretation that sees mountainous regions as areas of extremely incongruent weathering and high proportions of clay formation (e.g. Misra and Froelich, 2012). However, it is consistent with the 2D reactive transport model proposed by Fontorbe et al. (2013), in which clay formation is kinetically controlled, and also with the behaviour of lithium isotopes in uplifting areas (Pogge von Strandmann and Henderson, 2014). It is also consistent with mineralogical analyses of sediment carried by the Ganges in Himalayan streams: the clay size fraction is dominated (~80%) by detrital micas (Chakrapani et al., 1995), a major group of rock forming minerals. Only in the alluvial plain do authigenic clays become dominant components of the riverine clay minerals (Chakrapani et al., 1995). Finally, the interpretation that the alluvial plain is the chief locus of weathering and clay formation corroborates previous conclusions based on i) solute mass balance (Galy and France-Lanord, 1999) and ii) the geochemistry of sediments in the Bay of Bengal: progressive rain-out of the monsoon induces large latitudinal and longitudinal gradients in the O and H isotopic composition of rainwater, and clay assemblages since the late Miocene have O and H isotope ratios consistent with formation in

the palaeo-Gangetic plain (Derry and France-Lanord, 1996). Overall, some combination of low temperatures, low solute concentrations and short sediment and solution residence times combine to hinder secondary mineral formation in the mountainous regions. Seen the other way, the high solute concentrations and long sediment-water interaction times promote secondary clay formation and/or biological utilisation of DSi in the alluvial plain.

5.3. Mass balance, weathering and CO_2 consumption in the Ganges alluvial plain

Finally, an initial Si mobilisation rate (SMR, mol Si $km^{-2}\,yr^{-1}$) for rivers where discharge estimates are available, is simply the quotient of the observed Si yield, Y_{DSI} (mol Si $km^{-2}\,yr^{-1}$) and the calculated (unitless) $f_{Rayleigh}$ value:

$$SMR = Y_{DSi}/f_{Rayleigh} \quad (8)$$

and is shown in Table 2 for rivers of the Ganges basin. Normalised to catchment area, SMRs are lower in the GAP and peninsular rivers (107 and 150 kmol DSi $km^{-2}\,yr^{-1}$ respectively) than the Himalaya (200 kmol DSi $km^{-2}\,yr^{-1}$). Net DSi export (i.e. as observed in the river; Section 4.1.1 and Table 1) derives in a roughly 50/50 ratio from the Himalaya, and the plain and peninsular regions combined, in good agreement with previous work (Galy and France-Lanord, 1999). However, the initial release of Si during weathering, after accounting for reincorporation of Si into secondary phases following the approach above, is largely skewed towards the southern and alluvial plain catchments (Table 2) as a result of the (i) greater retention of Si and (ii) larger surface area. Our calculations (Table 2) suggest a total of c. 1300 Gmol Si yr^{-1} (i.e. $\sim 77 \times 10^6$ tons SiO_2 yr^{-1}) is initially mobilised within the Ganges basin, of which 24% derives from the Himalaya, 35% from the Indian Peninsula and 41% from the GAP. In other words, the majority of initial silicate weathering ($\sim$75%) takes place outside the mountains, consistent with the interpretation of West et al. (2002) on the basis of chemical to total denudation rates.

In terms of long-term CO_2 consumption via silicate weathering (Walker et al., 1981), the mobilisation of Si is unimportant – what matters is the release of silicate-hosted cations, predominantly Ca and Mg, and also Na and K to a lesser extent. The rationale for attempting to infer initial Si solubilisation rates is that if the Si–cation ratio of the source material is known, and provided it releases elements to solution congruently, Si isotope geochemistry potentially provides a powerful means of determining silicate-hosted Ca and Mg fluxes. As a first step, we assume the composition of sediment, bedload and banks in Himalayan Front rivers (Lupker et al., 2012) is representative of the material deposited in the GAP, These data suggest typical Ca/Si and Mg/Si molar ratios of $\sim$0.10 and $\sim$0.06, although the presence of detrital quartz or carbonate minerals will lower or increase, respectively, the cation/Si ratio of the silicate material susceptible to weathering. Crudely, our initial GAP Si mobilisation rate estimate of 55×10^9 mol Si yr^{-1} (Table 2) suggests that 5.5×10^9 mol Ca yr^{-1} and 3.3×10^9 mol Mg yr^{-1} are weathered from silicates in the GAP. These estimates overlap with those based on sediment composition change ($<10 \times 10^9$ mol yr^{-1} Ca and $17 \pm 23 \times 10^9$ mol yr^{-1} Mg, respectively) from Lupker et al. (2012), demonstrating that an Si-based approach can provide sensible values, and is readily improvable in future by i) more realistic silicate cation/Si ratios and ii) a better understanding of the processes determining the manifestation of Si isotope fractionation.

A growing body of work argues that the impact of Himalayan orogeny on global climate change is minimal since the surface area is small (Li et al., 2014; Moore et al., 2013). The work presented here adds another nuance to this argument: the presence of a vast alluvial plain with greater net weathering, albeit at lower weathering rates, means the influence of the Himalaya extends beyond their geographical boundaries (West et al., 2002). Although at the whole basin scale DSi export rates are relatively modest, they may still be greater than the situation before the onset of Himalayan orogenesis. The silicon isotopic composition of the Ganges very quickly loses its Himalayan character as it traverses the GAP, with the final DSi exported at Farrakah isotopically closer to Si derived from an alluvial plain source than a Himalayan source. Such lowland processes may also need to be considered in interpreting e.g. marine isotope curves for elements that dominantly reflect fractionation during weathering (e.g. Li) since the GAP has co-evolved with the Himalaya. Since the late Paleogene to early Neogene (Singh, 1996), downward flexing of the Indian plate after collision with Eurasia and subsequent sedimentary infilling has created the modern GAP. During its evolution, the sediment accommodation space, the rate and composition of sediment supply, and regional hydrology will inevitably have changed. These changes can have affected the capacity of the (palaeo-)GAP to store and weather Himalayan material, and thus the net weathering capacity attributable to the Himalayan orogeny will not have been constant. Some debate has focused on whether the Himalayan uplift hypothesis negates the possibility of a climate-weathering feedback. Since a majority of silicate weathering apparently occurs outside the Himalaya, this suggests that any climate-weathering feedback must operate primarily via the lowland regions.

6. Conclusions

At a whole-basin scale, the Ganges at Farrakah has dissolved Si yields (52 kmol $km^{-2}\,yr^{-1}$) and $\delta^{30}Si$ (1.93‰) similar to global average values (Section 4.1.1). The peninsular and alluvial plain tributaries have lower area-normalised silica-mobilisation rates than Himalaya rivers, but due to their larger surface area, the majority of Si mobilised during decomposition of primary minerals (75%) occurs outside the Himalaya. The contribution of the mountain vs. non-mountain to the measured net DSi export is approximately equal (i.e. 43% vs. 57%, respectively; Table 1) because a greater proportion of Si is retained in secondary phases in the alluvial plain and Indian shield catchments than in mountain catchments (Table 2). The basin-wide rate of silicate-weathering (and by extension, long-term CO_2 consumption), is therefore partially a function of whatever controls the supply of sediment to the alluvial plain, and the capacity of the alluvial plain to chemically weather this sediment. The co-evolution of the Himalayan orogeny and associated alluvial plains, together with hydrological changes that have occurred over the Neogene may have altered the efficiency and climate dependency of silicate weathering in the catchment.

Acknowledgements

This work was primarily funded by a grant from Lund Royal Physiographic Society (No. 31436) to PJF, plus support from the Knut and Alice Wallenberg Foundation to DJC and a LEFE/CYBER grant ("SiMS") to CDLR. We thank Carolina Funkey at Lund University for assistance with laboratory analysis, and the staff and students at IIT Roorkee for their help and enthusiasm. Julian Bouchez, Bastian Georg and an anonymous reviewer are thanked for their insightful comments on an earlier version of this manuscript.

Appendix A. Supplementary material

Supplementary material related to this article can be found online at http://dx.doi.org/10.1016/j.epsl.2015.06.049.

References

Berner, R.A., Caldeira, K., 1997. The need for mass balance and feedback in the geochemical carbon cycle. Geology 25, 955–956.

Bickle, M.J., Bunbury, J., Chapman, H.J., Harris, N.B.W., Fairchild, I.J., Ahmad, T., 2003. Fluxes of Sr into the headwaters of the Ganges. Geochim. Cosmochim. Acta 67, 2567–2584.

Bouchez, J., Gaillardet, J., Lupker, M., Louvat, P., France-Lanord, C., Maurice, L., Armijos, E., Moquet, J.-S., 2012. Floodplains of large rivers: weathering reactors or simple silos? Chem. Geol. 332–333, 166–184.

Bouchez, J., von Blanckenburg, F., Schuessler, J.A., 2013. Modeling novel stable isotope ratios in the weathering zone. Am. J. Sci. 313, 267–308.

Cardinal, D., Alleman, L.Y., de Jong, J., Ziegler, K., Andre, L., 2003. Isotopic composition of silicon measured by multicollector plasma source mass spectrometry in dry plasma mode. J. Anal. At. Spectrom. 18, 213–218.

Cardinal, D., Gaillardet, J., Hughes, H.J., Opfergelt, S., André, L., 2010. Contrasting silicon isotope signatures in rivers from the Congo Basin and the specific behaviour of organic-rich waters. Geophys. Res. Lett. 37, L12403.

Chakrapani, G.J., 2005. Major and trace element geochemistry in upper Ganga river in the Himalayas, India. Environ. Geol. 48, 189–201.

Chakrapani, G.J., Subramanian, V., Gibbs, R.J., Jha, P.K., 1995. Size characteristics and mineralogy of suspended sediments of the Ganges river, India. Environ. Geol. 25, 192–196.

Cockerton, H.E., Street-Perrott, F.A., Leng, M.J., Barker, P.A., Horstwood, M.S.A., Pashley, V., 2013. Stable-isotope (H, O, and Si) evidence for seasonal variations in hydrology and Si cycling from modern waters in the Nile Basin: implications for interpreting the Quaternary record. Quat. Sci. Rev. 66, 4–21.

Dalai, T.K., Krishnaswami, S., Sarin, M.M., 2002. Major ion chemistry in the headwaters of the Yamuna river system: chemical weathering, its temperature dependence and CO_2 consumption in the Himalaya. Geochim. Cosmochim. Acta 66, 3397–3416.

De La Rocha, C.L., Brzezinski, M.A., DeNiro, M.J., 1996. Purification, recovery, and laser-driven fluorination of silicon from dissolved and particulate silica for the measurement of natural stable isotope abundances. Anal. Chem. 68, 3746–3750.

De La Rocha, C.L., Brzezinski, M.A., DeNiro, M.J., 1997. Fractionation of silicon isotopes by marine diatoms during biogenic silica formation. Geochim. Cosmochim. Acta 61, 5051–5056.

Dellinger, M., Gaillardet, J., Bouchez, J., Calmels, D., Louvat, P., Dosseto, A., Gorge, C., Alanoca, L., Maurice, L., 2015. Riverine Li isotope fractionation in the Amazon River basin controlled by the weathering regimes. Geochim. Cosmochim. Acta 164, 71–93.

Delvaux, C., Cardinal, D., Carbonnel, V., Chou, L., Hughes, H.J., André, L., 2013. Controls on riverine δ^{30}Si signatures in a temperate watershed under high anthropogenic pressure (Scheldt–Belgium). J. Mar. Syst. 128, 40–51.

Derry, L.A., France-Lanord, C., 1996. Neogene Himalayan weathering history and river $^{87}Sr/^{86}Sr$: impact on the marine Sr record. Earth Planet. Sci. Lett. 142, 59–74.

Ding, T., Wan, D., Wang, C., Zhang, F., 2004. Silicon isotope compositions of dissolved silicon and suspended matter in the Yangtze River, China. Geochim. Cosmochim. Acta 68, 205–216.

Ding, T.P., Gao, J.F., Tian, S.H., Wang, H.B., Li, M., 2011. Silicon isotopic composition of dissolved silicon and suspended particulate matter in the Yellow River, China, with implications for the global silicon cycle. Geochim. Cosmochim. Acta 75, 6672–6689.

Dupuis, R., Benoit, M., Nardin, E., Méheut, M., 2015. Fractionation of silicon isotopes in liquids: the importance of configurational disorder. Chem. Geol. 396, 239–254.

Dürr, H.H., Meybeck, M., Hartmann, J., Laruelle, G.G., Roubeix, V., 2011. Global spatial distribution of natural riverine silica inputs to the coastal zone. Biogeosciences 8, 597–620.

Edmond, J., Huh, Y., 1997. Chemical weathering yields from basement and orogenic terrains in hot and cold climates. In: Ruddiman, W. (Ed.), Tectonic Uplift and Climate Change. Springer, US, pp. 329–351.

Engström, E., Rodushkin, I., Baxter, D.C., Öhlander, B., 2005. Chromatographic purification for the determination of dissolved silicon isotopic compositions in natural waters by high-resolution multicollector inductively coupled plasma mass spectrometry. Anal. Chem. 78, 250–257.

Engström, E., Rodushkin, I., Ingri, J., Baxter, D.C., Ecke, F., Osterlund, H., Ohlander, B., 2010. Temporal isotopic variations of dissolved silicon in a pristine boreal river. Chem. Geol. 271, 142–152.

Fontorbe, G., De La Rocha, C.L., Chapman, H.J., Bickle, M.J., 2013. The silicon isotopic composition of the Ganges and its tributaries. Earth Planet. Sci. Lett. 381, 21–30.

Frings, P., Clymans, W., Jeppesen, E., Lauridsen, T., Struyf, E., Conley, D., 2014. Lack of steady-state in the global biogeochemical Si cycle: emerging evidence from lake Si sequestration. Biogeochemistry 117, 255–277.

Frings, P.J., 2014. Integrating Fluvial Processes into the Global Si Cycle. Department of Geology, Lund University, Lund, p. 161.

Galy, A., France-Lanord, C., 1999. Weathering processes in the Ganges–Brahmaputra basin and the riverine alkalinity budget. Chem. Geol. 159, 31–60.

Georg, R.B., Reynolds, B.C., Frank, M., Halliday, A.N., 2006. Mechanisms controlling the silicon isotopic compositions of river waters. Earth Planet. Sci. Lett. 249, 290–306.

Georg, R.B., Reynolds, B.C., West, A.J., Burton, K.W., Halliday, A.N., 2007. Silicon isotope variations accompanying basalt weathering in Iceland. Earth Planet. Sci. Lett. 261, 476–490.

Georg, R.B., West, A.J., Basu, A.R., Halliday, A.N., 2009. Silicon fluxes and isotope composition of direct groundwater discharge into the Bay of Bengal and the effect on the global ocean silicon isotope budget. Earth Planet. Sci. Lett. 283, 67–74.

Hughes, H.J., Bouillon, S., André, L., Cardinal, D., 2012. The effects of weathering variability and anthropogenic pressures upon silicon cycling in an intertropical watershed (Tana River, Kenya). Chem. Geol. 308–309, 18–25.

Hughes, H.J., Sondag, F., Cocquyt, C., Laraque, A., Pandi, A., Andre, L., Cardinal, D., 2011. Effect of seasonal biogenic silica variations on dissolved silicon fluxes and isotopic signatures in the Congo River. Limnol. Oceanogr. 56, 551–561.

Hughes, H.J., Sondag, F., Santos, R.V., André, L., Cardinal, D., 2013. The riverine silicon isotope composition of the Amazon Basin. Geochim. Cosmochim. Acta 121, 637–651.

Jain, S., Agarwal, P., Singh, V., 2007. Ganga basin. In: Jain, S.K., Agarwal, P.K., Singh, V.P. (Eds.), Hydrology and Water Resources of India. Springer Netherlands, Dordecht, pp. 333–418.

Jarvis, A., Reuter, H., Nelson, A., Guevara, E., 2008. Hole-filled SRTM for the globe Version 4, available from the CGIAR-CSI SRTM 90m Database. http://srtm.csi.cgiar.org.

Kothyari, U., Garde, R., 1991. Annual runoff estimation for catchments in India. J. Water Resour. Plan. Manag. 117, 1–10.

Lehner, B., Doll, P., 2004. Development and validation of a global database of lakes, reservoirs and wetlands. J. Hydrol. 296, 1–22.

Lehner, B., Liermann, C.R., Revenga, C., Vörösmarty, C., Fekete, B., Crouzet, P., Döll, P., Endejan, M., Frenken, K., Magome, J., Nilsson, C., Robertson, J.C., Rödel, R., Sindorf, N., Wisser, D., 2011. High-resolution mapping of the world's reservoirs and dams for sustainable river-flow management. Front. Ecol. Environ. 9, 494–502.

Li, D.D., Jacobson, A.D., McInerney, D.J., 2014. A reactive-transport model for examining tectonic and climatic controls on chemical weathering and atmospheric CO_2 consumption in granitic regolith. Chem. Geol. 365, 30–42.

Lupker, M., France-Lanord, C., Galy, V., Lavé, J., Gaillardet, J., Gajurel, A.P., Guilmette, C., Rahman, M., Singh, S.K., Sinha, R., 2012. Predominant floodplain over mountain weathering of Himalayan sediments (Ganga basin). Geochim. Cosmochim. Acta 84, 410–432.

Misra, S., Froelich, P.N., 2012. Lithium isotope history of Cenozoic seawater: changes in silicate weathering and reverse weathering. Science 335, 818–823.

Moore, J., Jacobson, A.D., Holmden, C., Craw, D., 2013. Tracking the relationship between mountain uplift, silicate weathering, and long-term CO_2 consumption with Ca isotopes: Southern Alps, New Zealand. Chem. Geol. 341, 110–127.

Murnane, R.J., Stallard, R.F., 1990. Germanium and silicon in rivers of the Orinoco drainage-basin. Nature 344, 749–752.

Oelze, M., von Blanckenburg, F., Hoellen, D., Dietzel, M., Bouchez, J., 2014. Si stable isotope fractionation during adsorption and the competition between kinetic and equilibrium isotope fractionation: implications for weathering systems. Chem. Geol. 380, 161–171.

Opfergelt, S., Cardinal, D., André, L., Delvigne, C., Bremond, L., Delvaux, B., 2010. Variations of δ^{30}Si and Ge/Si with weathering and biogenic input in tropical basaltic ash soils under monoculture. Geochim. Cosmochim. Acta 74, 225–240.

Opfergelt, S., Cardinal, D., Henriet, C., Draye, X., André, L., Delvaux, B., 2006. Silicon isotopic fractionation by Banana (Musa spp.) grown in a continuous nutrient flow device. Plant Soil 285, 333–345.

Opfergelt, S., Delmelle, P., 2012. Silicon isotopes and continental weathering processes: assessing controls on Si transfer to the ocean. C. R. Géosci. 344, 723–738.

Pogge von Strandmann, P.A.E., Henderson, G.M., 2014. The Li isotope response to mountain uplift. Geology 43, 67–70.

Pokrovsky, O.S., Reynolds, B.C., Prokushkin, A.S., Schott, J., Viers, J., 2013. Silicon isotope variations in Central Siberian rivers during basalt weathering in permafrost-dominated larch forests. Chem. Geol. 355, 103–116.

Rai, S.K., Singh, S.K., Krishnaswami, S., 2010. Chemical weathering in the plain and peninsular sub-basins of the Ganga: impact on major ion chemistry and elemental fluxes. Geochim. Cosmochim. Acta 74, 2340–2355.

Raymo, M.E., Ruddiman, W.F., 1992. Tectonic forcing of late Cenozoic climate. Nature 359, 117–122.

Rengarajan, R., Singh, S.K., Sarin, M.M., Krishnaswami, S., 2009. Strontium isotopes and major ion chemistry in the Chambal River system, India: implications to silicate erosion rates of the Ganga. Chem. Geol. 260, 87–101.

Reynolds, B.C., Aggarwal, J., Andre, L., Baxter, D., Beucher, C., Brzezinski, M.A., Engstrom, E., Georg, R.B., Land, M., Leng, M.J., Opfergelt, S., Rodushkin, I., Sloane, H.J., van den Boorn, S., Vroon, P.Z., Cardinal, D., 2007. An inter-laboratory comparison of Si isotope reference materials. J. Anal. At. Spectrom. 22, 561–568.

Reynolds, B.C., Frank, M., Halliday, A.N., 2006. Silicon isotope fractionation during nutrient utilization in the North Pacific. Earth Planet. Sci. Lett. 244, 431–443.

Sarin, M.M., Krishnaswami, S., Dilli, K., Somayajulu, B.L.K., Moore, W.S., 1989. Major ion chemistry of the Ganga–Brahmaputra river system: weathering processes

and fluxes to the Bay of Bengal. Geochim. Cosmochim. Acta 53, 997–1009.
Savage, P.S., Georg, R.B., Williams, H.M., Halliday, A.N., 2013. The silicon isotope composition of the upper continental crust. Geochim. Cosmochim. Acta 109, 384–399.
Singh, I.B., 1996. Geological evolution of Ganga Plain – an overview.
Sinha, R., 2005. Why do Gangetic rivers aggrade or degrade? Curr. Sci. 89, 836.
Tripathy, G.R., Singh, S.K., 2010. Chemical erosion rates of river basins of the Ganga system in the Himalaya: reanalysis based on inversion of dissolved major ions, Sr, and $^{87}Sr/^{86}Sr$. Geochem. Geophys. Geosyst. 11, Q03013.
Walker, J.C.G., Hays, P.B., Kasting, J.F., 1981. A negative feedback mechanism for the long-term stabilization of earths surface-temperature. J. Geophys. Res., Oceans Atmos. 86, 9776–9782.
West, A.J., Bickle, M.J., Collins, R., Brasington, J., 2002. Small-catchment perspective on Himalayan weathering fluxes. Geology 30, 355–358.
White, A.F., Blum, A.E., 1995. Effects of climate on chemical-weathering in watersheds. Geochim. Cosmochim. Acta 59, 1729–1747.
Zachos, J., Pagani, M., Sloan, L., Thomas, E., Billups, K., 2001. Trends, rhythms, and aberrations in global climate 65 Ma to present. Science 292, 686–693.
Ziegler, K., Chadwick, O.A., Brzezinski, M.A., Kelly, E.F., 2005. Natural variations of $\delta^{30}Si$ ratios during progressive basalt weathering, Hawaiian Islands. Geochim. Cosmochim. Acta 69, 4597–4610.